Correlation of polishing-induced shallow subsurface damages with laser-induced gray haze damages in fused silica optics

Xiang He(何祥), Heng Zhao(赵恒), Gang Wang(王刚), Peifan Zhou(周佩璠), and Ping Ma(马平)†

Chengdu Fine Optical Engineering Research Center, Chengdu 610041, *China*

(Received 5 March 2016; revised manuscript received 15 April 2016; published online 25 June 2016)

Laser-induced damage in fused silica optics greatly restricts the performances of laser facilities. Gray haze damage, which is always initiated on ceria polished optics, is one of the most important damage morphologies in fused silica optics. In this paper, the laser-induced gray haze damages of four fused silica samples polished with CeO_2, Al_2O_3, ZrO_2, and colloidal silica slurries are investigated. Four samples all present gray haze damages with much different damage densities. Then, the polishing-induced contaminant and subsurface damages in four samples are analyzed. The results reveal that the gray haze damages could be initiated on the samples without Ce contaminant and are inclined to show a tight correlation with the shallow subsurface damages.

Keywords: laser-induced damage, polishing, subsurface damage, fused silica

PACS: 81.15.FG, 61.80.Ba, 81.65.Ps, 42.70.Ce **DOI:** 10.1088/1674-1056/25/8/088105

1. Introduction

The maximum output power of a high power laser facility is ultimately limited by the laser induced damage resistance of the optical components making up the system.[1] Pure fused silica as one of the most important optical materials has a wide bandgap and very high intrinsic laser-induced damage threshold.[2] However, even the highest quality optical components have lots of manufacturing-induced subsurface defects which restrict the damage resistance.[3,4] Once the damage happens in fused silica optics under 355-nm laser fluence, there are two distinctly different damage morphologies: the catastrophic damage and the gray haze damage.[5] The catastrophic damages represent the large single damage craters which have a typical width of tens of microns each.[6] Recent studies suggest that near-surface defects, such as absorptive contaminant and subsurface cracks are primarily responsible for initiating the catastrophic damages.[7–9] The gray haze damages, which are always initiated on the ceria polished surfaces, refer to the high-density pin-point damages with a typical width of ~ 1 μm.[10–12] The gray haze damages always occur at a low fluence compared with the catastrophic damages.[11] Moreover, the high-density gray haze damages can scatter light mightily and deteriorate the laser beam quality. It was indicated in Refs. [13]–[15] that eliminating the ceria polishing-induced redeposition layer, through either chemical etching or substitution of ZrO_2 polishing for ceria polishing, could reduce or remove the gray haze damages. However, in the present study, we find that the fused silica samples polished with different materials (CeO_2, Al_2O_3, ZrO_2, and colloidal silica) all present gray haze damages under a laser fluence. Combining hydrofluoric acid (HF) etching and differential interference contrast (DIC) microscopy reveals that the gray haze damages tend to show a tight correlation with the shallow subsurface damages.

2. Experiments

Four commercially available precisely polished UV-grade fused silica samples (labeled A, B, C, and D), each of which was 50 mm in diameter and 5 mm in thickness, were manufactured by different procedures. Firstly, four samples were etched in HF-based acid with a constant material removal of 20 μm per side to substantially eliminate (or expose) the previous subsurface damages.[16] Then, samples A, B, C, and D were precisely polished with commercially available CeO_2, Al_2O_3, ZrO_2, and colloidal silica slurries to remove a 10-μm-thick layer from each of their exit surfaces, respectively. All the polishing processes were performed under the same conditions such as pressure and rotation speed using a polishing cloth. The material removal rates of polishing with ceria (~ 2 μm/h), Al_2O_3 (~ 2 μm/h), ZrO_2 (~ 1 μm/h), and colloidal silica (~ 0.5 μm/h) slurries were different as a result of the different particle size distributions and chemical activities. Thus, four samples were polished for different times to achieve the same removal depth (10 μm in this text). To avoid cross contaminations of different slurries in the polishing process, a fresh polishing cloth was used to polish each sample. All samples were cleaned using the same multifrequency ultrasonic cleaning procedure prior to any tests. The size distributions of the polishing slurries were measured by a Zetasizer Nano ZS nano-particle analyzer. The average particle sizes of colloidal silica, ZrO_2, Al_2O_3, and CeO_2 were 60, 350, 860, and 980 nm, respectively. The surface roughness values of all samples were

†Corresponding author. E-mail: map@263.net

© 2016 Chinese Physical Society and IOP Publishing Ltd

measured with a white light interferometer. Samples A, B, C, and D presented the average surface roughness values of 1.2, 1.5, 0.9, and 0.7 nm RMS, respectively. Note that the colloidal silica slurry had the smallest average particle size while the ceria and Al_2O_3 slurry has the largest average particle size. It inclines to indicate that the larger polishing particle size causes the worst surface roughness, which is consistent with a previous result in Ref. [17]. The depth profiles of the contaminant elements in the redeposition layers were detected by a Model 2100 Trift II time-of-flight secondary ion mass spectrometry (TOF-SIMS).

A tripled Nd:YAG laser was used at a wavelength of 355 nm in the laser induced damage test equipment. The pulse is a single longitudinal mode with 5 ns (FWHM). During the test, the beam was focused on the exit surface to provide a near Gaussian beam with a diameter of about 0.7 mm at $1/e^2$ of maximum intensity. The damage threshold test was performed using the standard "1-on-1" test mode. The morphologies of the laser damages were recorded using a Leica DM4000M optical microscope. Raster scan damage test was used to estimate the gray haze damage density at a certain fluence and the scan area is about 10 mm^2 when considering the high density of the gray haze damages. Then the atomic force microscope (AFM) images of the gray haze damages were obtained to reveal the depth profile information.

After the previous measurements, all samples were etched 1um-thick layer from both sides in HF based acid to expose and widen the invisible subsurface damages. Since the DIC images are much more sensitive to small dots and shallow scratches than normal bright field images.[18] Combining HF etching and DIC images were used to analyze the subsurface damages in polished surfaces. To obtain the subsurface damage density, ten DIC images (650 μm×480 μm) of each sample are recorded at evenly spaced after the HF etching process by a Leica DM4000M optical microscope. The specific subsurface damage density was estimated as the ratio of the total number of the damages to the total area. The AFM images were captured to analyze the depths and widths of the subsurface damages. DIC images of the gray haze damages were also obtained after the HF etching process.

3. Results and discussions

The classic initial laser induced damage morphologies of the four samples are illustrated in Fig. 1. In Fig. 1, samples A and B show the similar damage morphologies which have a cluster of catastrophic damages in the center surrounded by the high density gray haze damages. Samples C and D also show some single catastrophic damages and gray haze damages. But the numbers (or densities) of the gray haze damages in samples C and D are much less than those in samples A and B. Table 1 presents the relative gray haze damage densities of four samples at a laser fluence of 15 J/cm^2. The vast difference between the orders of magnitude of the gray haze damage densities indicates that the damage precursors distributed in four samples have the much different densities and are tightly related to the polishing process. Figure 2 shows the AFM image and depth profile of the gray haze damages. The gray haze damages show a typical width of

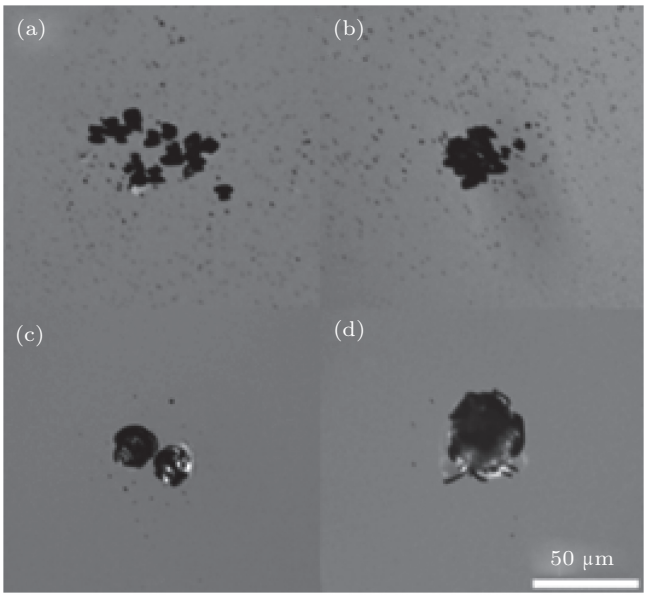


Fig. 1. Classic initial laser induced damage morphologies of samples (a) A, (b) B, (c) C at a laser fluence of 18 J/cm^2 and (d) D at a fluence of 22 J/cm^2. Note that sample D has the higher damage threshold (for catastrophic damages) than other samples.

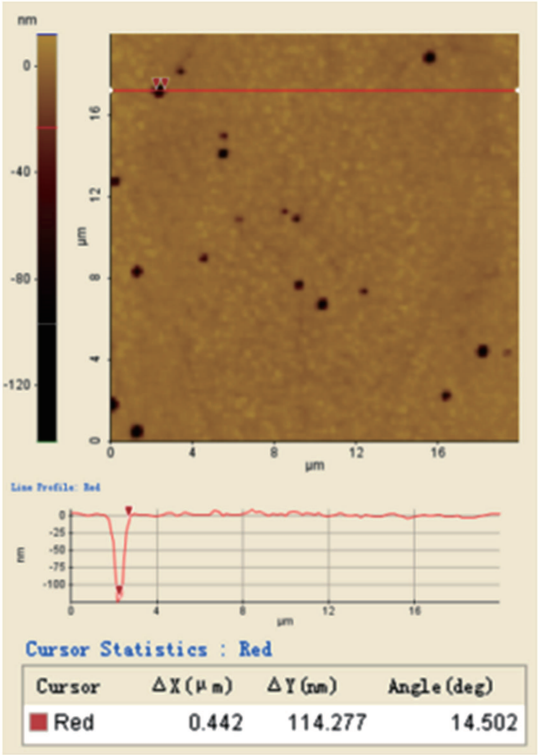


Fig. 2. (color online) AFM micrograph and depth profile (red line) of the gray haze damages in sample A.

$\sim$ 1 μm and typical depth of $\sim$ 100 nm. It is reasonable to deduce that the possible damage precursors for the gray haze damages are distributed in the outmost subsurface defect layer ($\sim$ 100 nm).

Table 1. Laser induced gray haze damage densities of four samples at a fluence of 15 J/cm^2.

Sample	Gray haze damages density/mm^2
A	1.3×10^4
B	0.94×10^4
C	1.8×10^2
D	24

The SIMS tests reveal that the main contaminant elements consist of Ce, Fe, Al, Zr, Cu, K, and Na. All of the contaminant elements show rapid decrease and disappear at the depth of 100 nm as usual, but the content values of the contaminant elements are much different from each other. The depth profile data are normalized with the silicon ion number (counts 10^4) as a standard for comparison. The cumulated relative amount of each element in the 100 nm redeposition layers is presented in Table 2. The Ce element is only found in sample A polished with CeO_2. The Zr element is only found in sample C polished with ZrO_2. All samples have Fe, Cu, and Al elements which are possibly induced by the polishing machine made of alloy. K and Na elements are possibly induced by the surfactant and pH regulator used in the polishing slurry. Since only sample A has Ce contaminant in the redeposition layer and sample B with no Ce contaminant also shows a high density of gray haze damages. It reveals that the gray haze damages could also be initiated on the samples without Ce contaminant in the redeposition layer. Some other defects besides Ce contaminant have produced the gray haze damages in samples B, C, and D.

Table 2. Cumulated quantities of each element in the redeposition layers of four samples.

Sample	Ce	Fe	Al	Zr	Cu	K	Na
A	420	112	1441	0	24	881	2123
B	0	132	4541	0	41	1354	1815
C	0	225	1851	636	87	3215	1328
D	0	96	241	0	15	3154	2215

To obtain the statistical distribution of the subsurface damages in full size, ten DIC images are recorded in each sample after the HF etching process. Many exposed subsurface damages such as continuous polishing scratches and polishing dots are clearly observed. Considering the fact that from each of these four fused silica samples has been removed a 20-μm-thick layer through HF etching prior to the final polishing process, most of the subsurface damages observed here should be produced in the final polishing process. For clarity of presentation, figure 3 shows the typical morphologies of the exposed subsurface damages in four samples. The continuous polishing scratches are marked by white squares. The polishing dots are marked by red circles. Figure 4 shows the AFM image and depth profile of the exposed subsurface damages in sample A after the HF etching process. The continuous polishing scratches and polishing dots show a typical depth of $\sim$ 10 nm and typical width of $\sim$ 0.3 μm. Note that sample A (Fig. 3(a)) and sample B (Fig. 3(b)) show lots of continuous polishing scratches and polishing dots. But sample C (Fig. 3(c)) presents much fewer continuous polishing scratches and polishing dots than samples A and B. Sample D only shows several polishing dots. Nearly no continuous polishing scratch is found in sample D. The density of the polishing dots and continuous polishing scratches in four samples are presented in Table 3. The density of the polishing dots is one order of magnitude higher than that of the scratches for all samples.

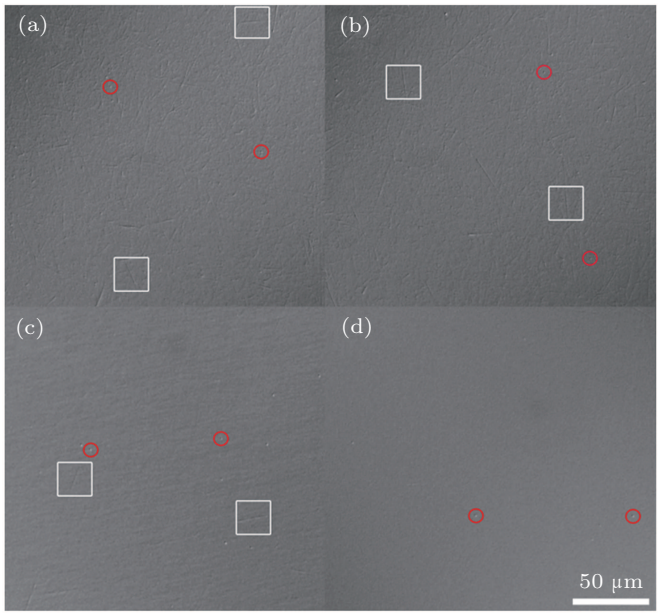


Fig. 3. (color online) Typical morphologies of the exposed subsurface damages in samples (a) A, (b) B, (c) C, and (d) D, after the HF etching process. The continuous polishing scratches are marked by white squares, and the polishing dots are marked by red circles.

Table 3. Polishing induced shallow subsurface damage densities of four samples.

Sample	Density of pits/mm^2	Density of scratches/mm^2
A	3.5×10^4	4.8×10^3
B	2.4×10^4	3.2×10^3
C	4.9×10^2	81
D	1.1×10^2	<1

The much different distributions of the shallow subsurface damages in four samples indicate that the formation of the subsurface damages tightly depends on the polishing parameters (particle size distribution). In the chemical mechanical polishing process, the main process composed of the formation of a soft hydrated layer and then the removal of the hydrated layer by abrasive particles.[19,20] So during the polishing, the loaded polishing particles would indent into the surface or plough up the surface to remove the materials,

which will form shallow polishing dots or continuous polishing scratches (as indicated in Fig. 4) through plastic flow. It is well admitted that the larger particle size would cause the higher loaded force per particle.[20–22] The higher loaded force per particle makes polishing particles more prone to creating scratches and dots. It possibly results in that sample D polished with colloidal silica only shows a few polishing dots (since the particle size of colloidal silica is much samller), sample C polished with ZrO_2 has much less polishing dots and scratches than samples A and B (considering the fact that samples A and B have the largest average particle sizes). Note that samples A and B show high-density catastrophic damage craters whereas samples C and D show very-low-density catastrophic damage craters as shown in Fig. 1. That is likely to be due to the fact that samples A and B have much more polishing induced subsurface damages than samples C and D. So the above results are inclined to indicate that the slurry particle size could possibly affect the polishing induced subsurface damages, and thus finally influence the laser induced damage performance.

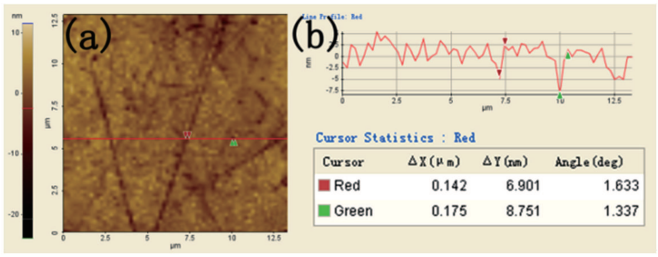


Fig. 4. (color online) (a) AFM image of the exposed subsurface damages in sample A after the HF etching process. (b) The depth profile of the red line in panel (a). The red and green cursor pairs indicate the continuous polishing scratches and polishing dot, respectively.

A comparison of Table 1 with Table 3 shows that the gray haze damage density increases with increasing the densities of the polishing dots and scratches. The densities of the gray haze damages and polishing dots have the same orders of magnitude in each sample. Figure 5 shows the DIC images of the gray haze damages in the four samples after the HF etching process. Some gray haze damages are directly initiated on the continuous polishing scratches, which are marked by yellow circles. These results tend to indicate that the shallow subsurface damages should have a great influence on the initiation of the gray haze damages. Actually, when the polishing particles indent into the surface to form the polishing dots (or scratches) in the polishing process, the tips of the particles are easy to crack and would possibly stay in the dots (or scratches), and finally be covered by a flowable hydrated layer ($\sim$ 100 nm) as invisible subsurface damages. Under a high power laser fluence, the tiny cracked polishing particles, even though they are transparent in bulk materials, could be the absorbers for UV laser.[23] In addition, the polishing dots (or scratches) could modulate the light intensity and enhance the field several times in some specific spots.[24–27] They all make these polishing dots (or scratches) damaged much more easily than a plane surface. That possibly causes the shallow polishing dots (or scratches) to show tight correlation with the gray haze damages.

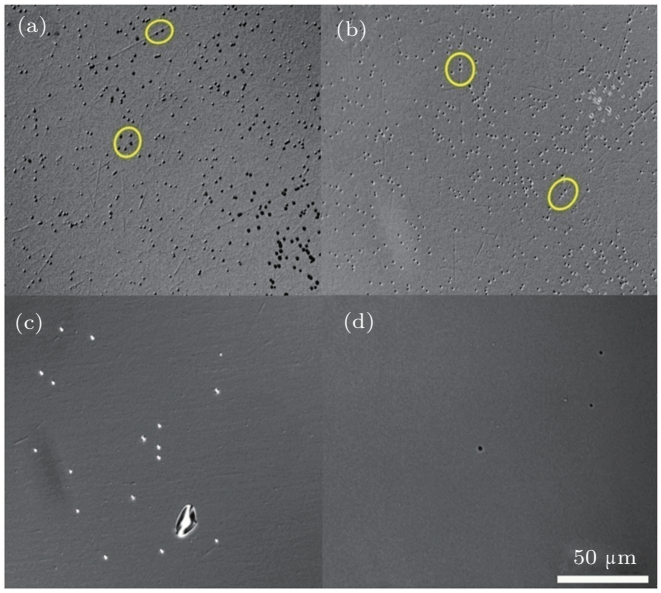


Fig. 5. (color online) Morphologies of the gray haze damages in samples (a) A, (b) B, (c) C, and (d) D after the HF etching process.

4. Conclusions

In this work, the laser induced gray haze damages with much different densities are found in fused silica optics polished with colloidal silica, ZrO_2, CeO_2, and Al_2O_3 slurries. The SIMS test proves that the gray haze damages could be initiated on the samples without Ce contaminant in the redeposition layer. Combining HF etching and DIC images is used to analyze the polishing-induced subsurface damages. It reveals that the densities of the polishing dots and the gray haze damages have the same orders of magnitude. The density of the gray haze damages increases with the densities of the polishing dots and scratches increasing. In addition, some gray haze damages are directly initiated on the continuous polishing scratches. Thus, the polishing-induced shallow subsurface damages are inclined to show a tight correlation with the initiation of the gray haze damages. These results can provide momentous support for further understanding the damage mechanism of gray haze damages.

Acknowledgment

The authors wish to thank Zheng Yi, Liu Zhichao and Ling Qi for laser-induced damage tests. The authors also thank Luo Jin for AFM tests.

References

[1] Huang W Q, Han W, Wang F, Xiang Y, Li F Q, Feng B, Jing F, Wei X F, Zheng W G and Zhang X M 2009 *Chin. Phys. Lett.* **26** 017901

[2] Stuart B C, Feit M D, Rubenchik A M, Shore B W and Perry M D 1995 *Phys. Rev. Lett.* **74** 2248

[3] Suratwala T, Wong L, Miller P, Feit M D, Menapace J, Steele R, Davis P, and Walmer D 2006 *J. Non-Cryst. Solids* **352** 5601

[4] Miller P E, Suratwala T I, Wong L L, Feit M D, Menapace J A, Davis P J and Steele R A 2005 *Proc. SPIE* **5991** 599101

[5] Genin F Y, Sheehan L, Yoshiyama J, Dijon J and Garrec P 1998 *Proc. SPIE* **3244** 155

[6] Wong J, Ferriera J L, Lindsey E F, Haupt D L, Hutcheon I D and Kinney J H 2006 *J. Non-Cryst. Solids* **352** 255

[7] Miller P E, Suratwala T I, Bude J D, Laurence T A, Shen N, Steele W A, Feit M D, Menapace J A and Wong L L 2009 *Proc. SPIE* **7504** 75040X

[8] Miller P E, Bude J D, Suratwala T I, Shen N, Laurence T A, Steele W A, Menapace J, Feit M D and Wong L L 2010 *Opt. Lett.* **35** 2702

[9] Bercegol H, Grua P, Hebert D and Morreeuw J P 2007 *Proc. SPIE* **6720** 672003

[10] Genin F Y, Campbell J, Yoshiyama J, Salleo A and Sands T 1998 *Proc. SPIE* **3244** 348

[11] Camp D W, Kozlowski M R, Sheehan L M, Nichols M, Dovik M, Raether R and Thomas I 1998 *Proc. SPIE* **3244** 356

[12] Neauport J, Lamaignere L, Bercegol H, Pilon F and Birolleau J C 2005 *Opt. Express* **13** 10163

[13] Sheehan L M, Kozlowski M and Camp D W 1998 *Proc. SPIE* **3244** 282

[14] Yoshiyama J, Genin F Y, Salleo A, Thomas I, Kozlowski M R, Sheehan L M, Hutcheon I D and Camp D W 1998 *Proc. SPIE* **3244** 331

[15] Kozlowski M R, Carr J, Hutcheon I, Torres R, Sheehan L, Camp D and Yan M 1998 *Proc. SPIE* **3244** 365

[16] Liu H J, Ye X, Zhou X D, Huang J, Wang F R, Zhou X Y, Wu W D, Jiang X D, Sui Z and Zheng W G 2014 *Opt. Mater.* **36** 855

[17] Suratwala T, Feit M, Steele W, Wong L, Shen N, Dylla-Spears R, Desjardin R, Mason D, Geraghty P, Miller P and Baxamusa S 2014 *J. Am. Ceram. Soc.* **97** 81

[18] He X, Wang G, Zhao H and Ma P 2016 *Chin. Phys. B* **25** 048104

[19] Tomozawa M 1997 *Solid State Technol.* **40** 169

[20] Evans C J, Paul E, Dornfeld D, Lucca D A, Byrne G, Tricard M, Klocke F, Dambon O and Mullany B A 2003 *CIRP Ann-Manuf. Technol.* **52** 611

[21] Jeng Y R and Huang P Y 2004 *Electrochem. Solid State Lett.* **7** G40

[22] Liao D F, Wang J, Zhao S J, Xie R Q, Chen X H, Yuan Z G, Zhong B, Xu X and Zhang S 2014 *J. Non-Cryst. Solids* **391** 96

[23] Bude J, Miller P, Baxamusa S, Shen N, Laurence T, Steele W, Suratwala T, Wong L, Carr W, Cross D and Monticelli M 2014 *Opt. Express* **22** 5839

[24] Zhang L, Chen W and Hu L L 2013 *Appl. Opt.* **52** 980

[25] Feit M D and Rubenchik A M 2004 *Proc. SPIE* **5273** 264

[26] Zhang C L, Yuan X D, Xiang X, Wang Z G, Liu C M, Li L, He S B and Zu X T 2012 *Chin. Phys. B* **21** 094213

[27] Li L, Xiang X, Zu X T, Wang H J, Yuan X D, Jiang X D, Zheng W G and Dai W 2011 *Chin. Phys. B* **20** 074209